Journal of
Synchrotron Radiation

ISSN 0909-0495

Received 22 June 2009
Accepted 16 November 2009

Synchrotron-based X-ray diffraction of the lead apatite series $Pb_{10}(PO_4)_6Cl_2$–$Pb_{10}(AsO_4)_6Cl_2$

Justyna Flis,[a]* Olaf Borkiewicz,[b] Tomasz Bajda,[a] Maciej Manecki[a] and Jolanta Klasa[a]

[a]Department of Mineralogy, Petrography and Geochemistry, AGH-University of Science and Technology, Al. Mickiewicza 30, 30-059 Cracow, Poland, and [b]Department of Geology, Miami University, Oxford, OH 45056, USA. E-mail: flisjustyna@tlen.pl

A number of compounds of the pyromorphite–mimetite solid solution series were synthesized at room temperature and analyzed with infrared spectroscopy and powder X-ray diffraction. High-resolution high-quality powder diffraction data were obtained by means of the state-of-the-art instrument at the 11-BM beamline of the Advanced Photon Source at Argonne National Laboratory, Argonne, IL, USA. The unit-cell dimensions, atomic position and atomic displacement parameters, as well as site occupancy for analyzed phases, were refined by the Rietveld method and reported herein for the first time. The results of this study indicate that the pyromorphite–mimetite series is continuous in near-Earth-surface environments. Detailed structural changes caused by P^{5+}–As^{5+} substitutions in minerals from the pyromorphite–mimetite solid solution series are reported.

Keywords: apatites; solid solutions; diffraction; Rietveld refinement.

1. Introduction

Pyromorphite $Pb_{10}(PO_4)_6Cl_2$ and mimetite $Pb_{10}(AsO_4)_6Cl_2$, members of the apatite group minerals, have recently gained considerable attention as metal sequestration agents in water treatment and contaminated soil remediation (*e.g.* Ma *et al.*, 1993; Ruby *et al.*, 1994). The unique crystal structure and chemistry of these minerals allow for numerous substitutions of both metal cations and anionic complexes (Pan & Fleet, 2002). The vast majority of studies conducted to date, however, have focused on the cationic substitutions in these minerals. Little is known about the response of the structure to anionic substitutions, which may also influence properties, stability and environmental behaviour of studied apatites. Natural pyromorphite and mimetite often exhibit a certain degree of anionic substitutions, which suggests relative stability of their solid solutions in natural environments (Nakamoto *et al.*, 1969). From diffraction studies on the mimetite–pyromorphite series synthesized at high temperatures it has been found that the solid solution between these two end members is complete (Baker, 1966; Masaoka *et al.*, 2006). The temperature of the synthesis, however, renders the obtained data inapplicable to near-Earth-surface environments. In order to supplement existing data, a number of compounds covering a wide range of compositions between pyromorphite–mimetite end members were synthesized at room temperature. Precipitated crystals were analyzed by synchrotron-based X-ray diffraction. Owing to the use of the state-of-the-art instrument at the dedicated powder diffraction beamline at the Advanced Photon Source (Wang *et al.*, 2008), high-resolution high-quality powder diffraction data were obtained and the first structure Rietveld refinements of minerals from the pyromorphite–mimetite series were provided.

2. Experimental

2.1. Synthesis

In order to study the pyromorphite–mimetite solid solution series as nanocrystals forming in near-Earth-surface environments, pure pyromorphite $Pb_{10}(PO_4)_6Cl_2$, mimetite $Pb_{10}(AsO_4)_6Cl_2$ and nine minerals with intermediate compositions $Pb_{10}(BO_4)_6Cl_2$, where B = As + P, of various P/As ratios were synthesized at 298 K. Synthesis of the solids was carried out by dropwise mixing of aqueous solutions of $Pb(NO_3)_2$, KCl and/or K_2HPO_4 and/or $Na_2HAsO_4{\cdot}7H_2O$ in molar proportions based on the stoichiometry of the phases [Pb:P:Cl = 5:3:1, Pb:As:Cl = 5:3:1 and Pb:(P + As):Cl = 5:3:1]. Suspensions of the forming precipitates were stirred using a mechanical stirrer for 5 h and were allowed to settle. After two weeks of reactions the precipitates were separated from the solutions by decantation. Then they were washed thoroughly several times with redistilled water and acetone and dried at 383 K.

2.2. Preliminary solid characterization

The synthetic solids were analyzed using scanning electron microscopy (SEM) coupled with energy-dispersive spectroscopy (EDS) and infrared spectroscopy. Additionally, seven out of 11 solids were characterized by wet chemical analysis. SEM-EDS examinations were conducted using Jeol 5200 and FEI QUANTA 200 FEG instruments at 25 kV and 20 kV, respectively. Infrared spectra were measured on a Bio-Rad FTS-60 spectrometer. Spectra were collected in the mid- and far-infrared region (4000–400 cm^{-1}) after 256 scans at 2 cm^{-1} resolution. Samples were prepared by the standard KBr and polyethylene (Merck) pellets method. Small amounts of the pyromorphite, mimetite and five of their solid solutions were digested in 0.02 *M* EDTA and analysed for Pb using atomic absorption spectroscopy and for P and As using the colourimetric method of Lenoble *et al.* (2003).

2.3. High-resolution X-ray diffraction

Powders were grinded using pestle and mortar and sieved through a 20 µm sieve. On average 2.5 mg of the samples were loaded into a Kapton tube, sealed and mounted on bases provided by the 11-BM beamline of the Advanced Photon Source. A set of samples was mailed to the Advanced Photon Source for analysis. The diffraction experiments were carried out at room temperature using monochromatic synchrotron radiation of wavelength 0.4015 Å. The intensities of the diffracted X-rays were collected on a unique 12-element Si (111) crystal analyzer/detector system offering supreme resolution and greatly reduced data collection time. A robotic sample changer was used allowing for quick and precise sample exchange and high-throughput data collection. Raw data from each of the 12 detectors were calibrated, merged and reduced using in-house routines (Lee *et al.*, 2008).

The full width at half-maximum (FWHM) of the three most intense diffraction peaks (112, 211, 300) for all members of the solid solution series has been derived from diffraction data using peak profile fitting procedures implemented in data analysis software *Jade 7.0* (Materials Data Inc.). The instrumental FWHM at the appropriate 2θ range was taken from Wang *et al.* (2008) and a linear background was used during fitting procedures. An error of 5% or less was achieved for all analyzed samples.

2.4. Structural Rietveld refinement of the acquired data

All refinements were performed using the *General Structure Analysis System (GSAS)* program of Larson & Von Dreele (2000) using the *EXPGUI* interface of Toby (2001). The starting parameters for mimetite and pyromorphite structures were taken from Dai *et al.* (1991) and Dai & Hughes (1989), respectively. The refinement parameters included the scale factor and 30 to 36 background terms in a Chebyshev first-order polynomial. Peak profiles were modelled with a pseudo-Voigt profile function as parameterized by Thompson *et al.* (1987) with asymmetry corrections from Finger *et al.* (1994) and microstrain anisotropic broadening terms from Stephens (1999). The unit-cell dimensions were refined after convergence for the aforementioned parameter was achieved. Then atomic positions, occupancy factors and isotropic atomic displacement factors were varied.

3. Results and discussion

3.1. Preliminary solid characterization

All experiments carried out as part of this study yielded white homogeneous precipitates. Examination by SEM-EDS revealed particles ranging from 1 to 5 µm in size and containing Pb, P, O, Cl and/or As as major constituents. Figs. 1(*a*), 1(*b*) and 1(*c*) present SEM images of pyro-

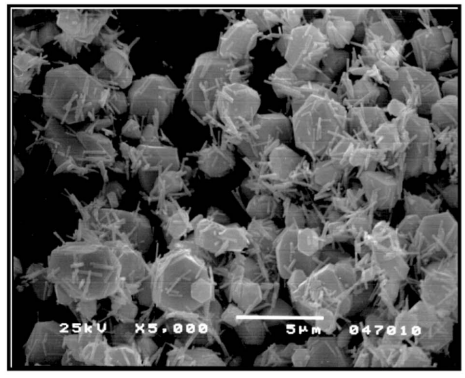

(*a*)

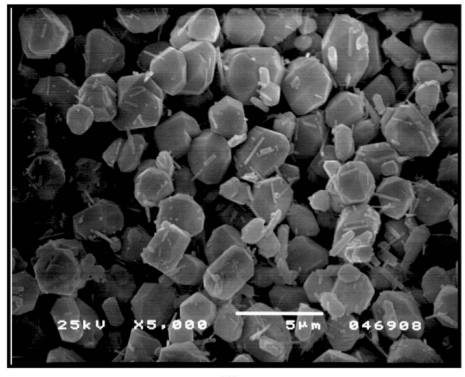

(*b*)

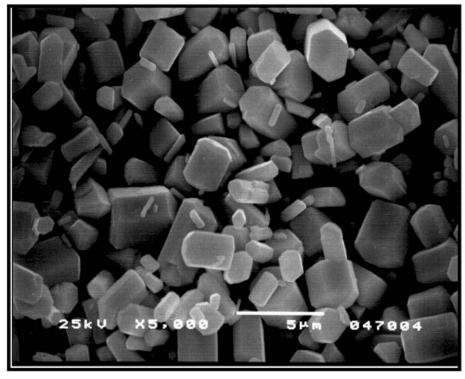

(*c*)

Figure 1
SEM microphotographs of selected synthesized precipitates: (*a*) pyromorphite $Pb_{10}(PO_4)_6Cl_2$, (*b*) solid solution $Pb_{10}(PO_4)_3(AsO_4)_3Cl_2$ and (*c*) mimetite $Pb_{10}(AsO_4)_6Cl_2$.

morphite $Pb_{10}(PO_4)_6Cl_2$, intermediate solid solution member $Pb_{10}(PO_4)_3(AsO_4)_3Cl_2$ and mimetite $Pb_{10}(AsO_4)_6Cl_2$, respectively. Typical for apatites, morphology in the form of hexagonal prisms was observed. No secondary crystalline or amorphous phases were detected. The results of EDS and wet chemical analysis of the solids are presented in Table 1. The analysis yielded compositions of the precipitates very close to the intended model chemistry of compounds of interest. The deviations from the ideal formulas are within the average analytical error estimated by triplicates, at 95% confidence level to 5%. The proposed method of synthesis of minerals from the pyromorphite–mimetite solid solution series for environmental research purposes appeared to be successful. In order to simplify identification of the particular members of the solid solution in this paper, the theoretical-intended As/(P + As) ratio in analysed solids was used as the sample ID (Table 1).

Table 1
Results of the SEM-EDS and wet chemical analysis of the solids precipitated during the synthesis.

Sample ID intended As/(P + As)	Intended sample composition	Sample composition by SEM-EDS analysis	Sample composition by wet chemical analysis
0	$Pb_{10}(PO_4)_{6.0}Cl_2$	$Pb_{10}(PO_4)_{6.0}Cl_2$	$Pb_{10.18}(PO_4)_{5.92}Cl_2$†
0.1	$Pb_{10}(PO_4)_{5.4}(AsO_4)_{0.6}Cl_2$	$Pb_{10}(PO_4)_{5.22}(AsO_4)_{0.66}Cl_2$	–
0.2	$Pb_{10}(PO_4)_{4.8}(AsO_4)_{1.2}Cl_2$	$Pb_{10}(PO_4)_{4.68}(AsO_4)_{1.14}Cl_2$	$Pb_{10.22}(PO_4)_{4.76}(AsO_4)_{1.12}Cl_2$
0.3	$Pb_{10}(PO_4)_{4.2}(AsO_4)_{1.8}Cl_2$	$Pb_{10}(PO_4)_{4.14}(AsO_4)_{1.74}Cl_2$	$Pb_{10.04}(PO_4)_{4.26}(AsO_4)_{1.7}Cl_2$
0.4	$Pb_{10}(PO_4)_{3.6}(AsO_4)_{2.4}Cl_2$	$Pb_{10}(PO_4)_{3.48}(AsO_4)_{2.4}Cl_2$	–
0.5	$Pb_{10}(PO_4)_{3.0}(AsO_4)_{3.0}Cl_2$	$Pb_{10}(PO_4)_{2.82}(AsO_4)_{2.94}Cl_2$	$Pb_{10.34}(PO_4)_{2.9}(AsO_4)_{2.94}Cl_2$
0.6	$Pb_{10}(PO_4)_{2.4}(AsO_4)_{3.6}Cl_2$	$Pb_{10}(PO_4)_{2.34}(AsO_4)_{3.54}Cl_2$	–
0.7	$Pb_{10}(PO_4)_{1.8}(AsO_4)_{4.2}Cl_2$	$Pb_{10}(PO_4)_{1.8}(AsO_4)_{4.14}Cl_2$	$Pb_{10.56}(PO_4)_{1.66}(AsO_4)_{4.08}Cl_2$
0.8	$Pb_{10}(PO_4)_{1.2}(AsO_4)_{4.8}Cl_2$	$Pb_{10}(PO_4)_{1.08}(AsO_4)_{4.8}Cl_2$	$Pb_{10.74}(PO_4)_{1.04}(AsO_4)_{4.64}Cl_2$
0.9	$Pb_{10}(PO_4)_{0.6}(AsO_4)_{5.4}Cl_2$	$Pb_{10}(PO_4)_{0.54}(AsO_4)_{5.34}Cl_2$	–
1	$Pb_{10}(AsO_4)_{6.0}Cl_2$	$Pb_{10}(AsO_4)_{6.0}Cl_2$	$Pb_{10.56}(AsO_4)_{6.38}Cl_2$

† Cl ions assumed based on ideal formula of mineral.

Table 2
Band assignments (cm^{-1}) of As—O and P—O complexes in minerals from the pyromorphite–mimetite series.

	Sample ID										
Modes	0	0.1	0.2	0.3	0.4	0.5	0.6	0.7	0.8	0.9	1
ν_1 As—O	–	–	–	–	–	–	–	–	–	–	–
ν_1 P—O	926	924	924	922	922	922	922	920	920	920	–
ν_2 As—O	–	–	–	–	–	–	–	–	–	–	–
ν_2 P—O	436	434	436	436	438	436	433	–	–	–	–
ν_{3a} As—O	–	789	789	787	787	787	789	787	787	787	783
ν_{3b} As—O		803	801	801	801	803	804	804	804	804	804
ν_{3c} As—O		818	816	814	812	810	812	814	814	812	814
ν_{3a} P—O	972	970	967	963	961	961	961	957	957	955	–
ν_{3b} P—O	998	996	994	992	996	996	988	990	986	986	
ν_{3c} P—O	1032	1026	1019	1014	1007	1002	1007	1000	1005	1005	
ν_{4a} As—O	–	380	375	375	372	370	371	370	368	370	375
ν_{4b} As—O		424	422	420	418	418	418	414	414	412	410
ν_{4a} P—O	–	540	542	542	542	542	542	541	540	540	
ν_{4b} P—O		–	–	–	–	–	–	550	550	552	
ν_{4c} P—O		573	573	571	571	571	569	569	569	567	

In the mid-infrared spectral region, bands attributable to phosphate and arsenate anions can be observed. The spectra of the mimetite–pyromorphite solid solution are complex with the spectral profile in the 900–400 cm^{-1} region. Infrared spectra were poorly defined in the 3600–1500 cm^{-1} region and are excluded from consideration. The observation of isomorphic substitution between $(PO_4)^{3-}$ and $(AsO_4)^{3-}$ could easily be distinguished on the basis of their spectral properties from the mixed spectra of phosphate and arsenate ions in the solid solution series. IR spectra of pyromorphite show characteristic bands originating from the vibrations of P—O bonds present in $[PO_4]$ tetrahedra (Table 2). These are the bands due to stretching ν_1 (926 cm^{-1}) and ν_3 modes (1032, 998, 972 cm^{-1}) as well as bands originating from bending ν_4 (575, 540 cm^{-1}) and ν_2 modes (436 cm^{-1}) occurring within these units. The number of bands due to $(PO_4)^{3-}$ tetrahedra vibrations (Nakamoto, 1986) indicates lowering of their symmetry from the T_d point group to the C_{2v} group. Gradual substitution of $(PO_4)^{3-}$ anions with $(AsO_4)^{3-}$ in the analyzed solid solution structures results in changes in the number of bands as well as in their positions. An increase in the number of bands originating from bending asymmetric modes ν_4 is observed. The profile of the ν_4 absorption varies with composition and the band splitting increases from pyromorphite to mimetite. This is due to the increasing distortion of the phosphate ion in this direction. The substitutions of $(AsO_4)^{3-}$ for $(PO_4)^{3-}$ in the pyromorphite–mimetite series cause a decrease in the vibrational frequencies of ν_3 and ν_1 modes of $(PO_4)^{3-}$ to lower wavenumbers. The same dependence was observed in the natural arsenian pyromorphite (Frost *et al.*, 2008). The regular changes in the positions of the ν_{3a} band, owing to $(PO_4)^{3-}$ tetrahedra vibrations, with composition of the solid solution (Table 2) can be used as an indicator of the phosphate content in the pyromorphite–mimetite solid solution series. IR spectra of mimetite contain characteristic bands resulting from deformational vibrations of $(AsO_4)^{3-}$ tetrahedra (Table 2). These are the bands due to stretching ν_3 modes (814, 804, 783 cm^{-1}) as well as the bands at 375 and 410 cm^{-1} originating from the bending ν_4 mode occurring within these units. Gradual substitution of $(AsO_4)^{3-}$ anions with $(PO_4)^{3-}$ in the structure of the analyzed solid solutions does not generally change the number or the position of the bands. The band at 410 cm^{-1} is shifted slightly to higher wavenumbers; however, the dependency is not linear. The lack of variation in the position of the bands indicates no change in the local symmetry of the arsenate tetrahedron within the series. Comparison of the number of bands resulting from the $(AsO_4)^{3-}$ tetrahedra vibrations (Nakamoto *et al.*, 1969) with

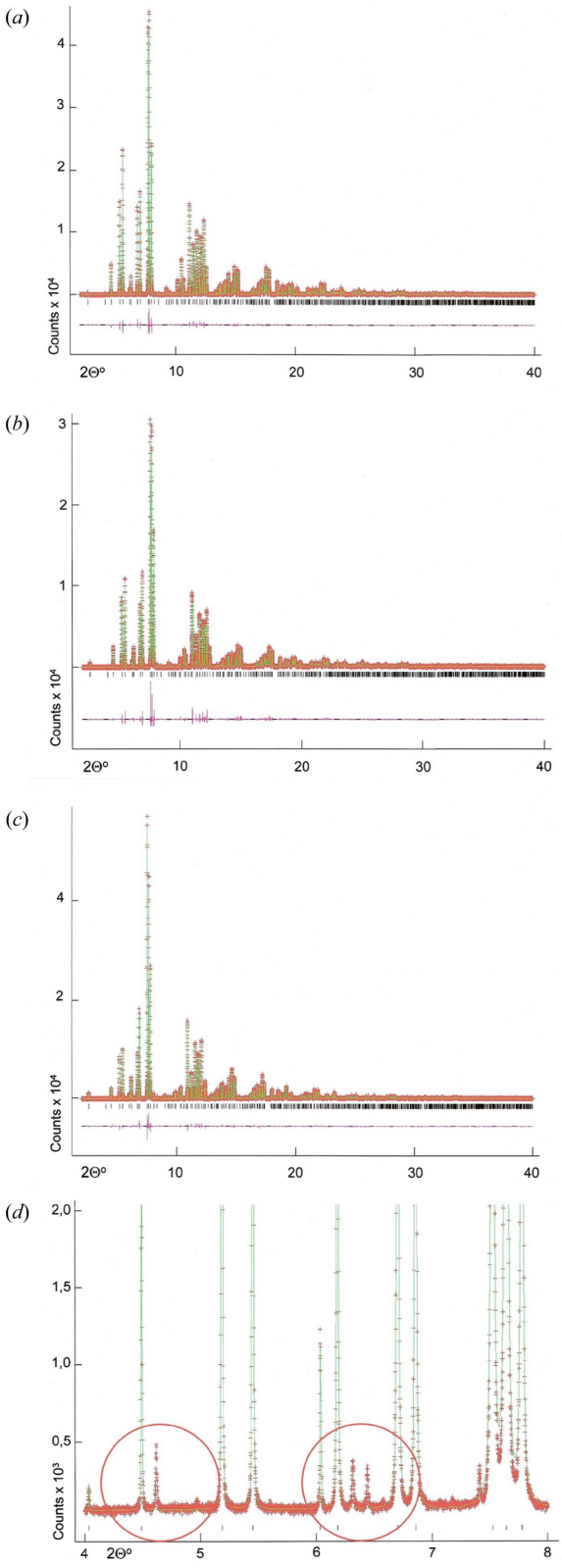

Figure 2
Final observed, collected and difference powder diffraction patterns for the Rietveld refinement of selected synthesized precipitates: (*a*) pyromorphite $Pb_{10}(PO_4)_6Cl_2$, (*b*) solid solution $Pb_{10}(PO_4)_3(AsO_4)_3Cl_2$ and (*c*) mimetite $Pb_{10}(AsO_4)_6Cl_2$. (*d*) Mimetite $Pb_{10}(AsO_4)_6Cl_2$ close-up of the region of interest containing additional peaks previously undetected (red circles).

the correlation scheme of the $(AsO_4)^{3-}$ anion indicates that its symmetry is lowered from T_d to C_{2v} point group.

3.2. High-resolution X-ray diffraction

The use of the dedicated high-resolution high-throughput diffraction beamline 11-BM allowed for quick collection of data of a quality unavailable on any conventional radiation source. The typical collection time under the conditions used is roughly 1 h per sample. Final observed, calculated and difference powder diffraction patterns for Rietveld refinement of selected minerals from the pyromorphite–mimetite series are presented in Fig. 2. All analyzed phases were identified as pyromorphite, mimetite and their solid solutions. A variation in (300) spacing with chemical composition was observed. The greater the As^{5+} content in the analyzed sample, the lower the diffraction 2θ angle for (300) spacing measured. This peak shift was also observed in previous studies (Baker, 1966; Masaoka *et al.*, 2006), in which the pyromorphite–mimetite solid solution series was confirmed to be continuous at high temperatures. Characteristics of the synchrotron radiation allowed also for the detection of minor impurities in the analyzed precipitates. Observed impurities were undetectable by other methods. In the X-ray patterns of phases with an As/(As + P) ratio greater than 0.5, some additional peaks were distinguished (Fig. 2*d*). These unidentified peaks appear within the whole range of 2θ. The impurities might be an effect of a synthesis or a simple contamination. However, interpretation of the impurities was not the objective of this study. Intensities of the additional peaks are negligible and their positions are clear. Some overlapping within peaks of impurities and those of pyromorphite–mimetite phases was observed. Nevertheless, the Rietveld refinement and structural interpretation of the pyromorphite–mimetite phases were successfully performed.

The FWHM of the three most intense X-ray diffraction peaks plotted as a function of chemical composition of the pyromorphite–mimetite solid solution members is presented in Fig. 3. The standard deviation of the derived FWHM values

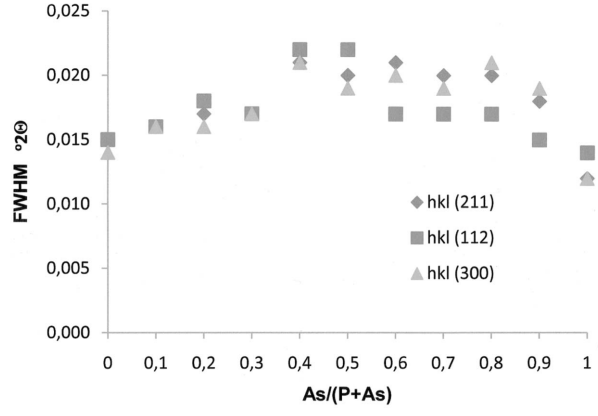

Figure 3
FWHM for selected X-ray diffraction peaks as a function of chemical composition of minerals from the pyromorphite–mimetite series.

Table 3
Summary of the results of structural Rietveld refinement of minerals from the pyromorphite–mimetite series.

Sample ID	wR_p/R_p	χ^2	Unit-cell dimensions a/c (Å)	Refined composition
0	0.08/0.06	2.098	9.9938 (01)/7.3397 (01)	$Pb_{10}(PO_4)_{6.04}Cl_2$
0.1	0.09/0.07	1.983	10.0186 (03)/7.3501 (02)	$Pb_{10}(PO_4)_{5.43}(AsO_4)_{0.57}Cl_2$
0.2	0.10/0.08	1.818	10.0441 (05)/7.3607 (05)	$Pb_{10}(PO_4)_{4.86}(AsO_4)_{1.14}Cl_2$
0.3	0.09/0.07	3.491	10.0720 (03)/7.3696 (04)	$Pb_{10}(PO_4)_{4.21}(AsO_4)_{1.79}Cl_2$
0.4	0.11/0.08	2.055	10.0989 (04)/7.3833 (04)	$Pb_{10}(PO_4)_{3.67}(AsO_4)_{2.33}Cl_2$
0.5	0.097/0.076	2.701	10.1236 (04)/7.3985 (03)	$Pb_{10}(PO_4)_{2.98}(AsO_4)_{3.02}Cl_2$
0.6	0.092/0.071	2.866	10.1496 (01)/7.4164 (02)	$Pb_{10}(PO_4)_{2.36}(AsO_4)_{3.64}Cl_2$
0.7	0.094/0.074	2.860	10.1757 (02)/7.4241 (02)	$Pb_{10}(PO_4)_{1.75}(AsO_4)_{4.25}Cl_2$
0.8	0.110/0.086	4.290	10.2035 (02)/7.4396 (02)	$Pb_{10}(PO_4)_{1.03}(AsO_4)_{4.97}Cl_2$
0.9	0.112/0.088	4.428	10.2239 (02)/7.4461 (02)	$Pb_{10}(PO_4)_{0.53}(AsO_4)_{5.47}Cl_2$
1	0.096/0.070	3.371	10.2518 (02)/7.4482 (02)	$Pb_{10}(AsO_4)_{6.08}Cl_2$

is depicted by the size of the data point markers. The apparent increase in peak FWHM for samples with intermediate (the most diverse) composition may indicate a growing disorder in the structure of the corresponding solid solution members. The disorder may be explained by the rising number of substituting anions and consequent diversification/deterioration of the structure (Rajan & Lim, 2003). These findings are in good agreement and are supported by the results of IR spectroscopy analyses of the solids (not shown). Although the particle size, determined by SEM to be around 5 µm, seems to be consistent along the series, formation of nanocrystals contributing to the increase in the FWHM cannot be ruled out.

3.3. Rietveld refinement

The atomic positions and atomic displacement parameters as well as site occupancy and unit-cell dimensions of pyromorphite, mimetite and intermediate members of the solid solutions have been refined to mean wR_p/R_p = 0.10/0.076 and χ^2 = 2.94. The final refinement parameters for each phase along with refined cell constants and chemical compositions are listed in Table 3. The atomic coordinates and equivalent isotropic displacement factors for 11 analyzed mineral phases are listed in Table 4. Selected bond lengths and angles are included in Table 5. This study reports first to date structure refinement of the intermediate members of the pyromorphite–mimetite solid solution series. Thus, only the pyromorphite and mimetite structures have been referenced and compared with previously reported data. The atomic arrangements of pyromorphite and mimetite as determined, respectively, by Dai & Hughes (1989), Calos & Kennard (1990) and Dai *et al.* (1991) have been confirmed in principle. Our mean Pb—O and *B*—O bond lengths as well as particular O—*B*—O bond angles agree with theirs within 0.04 Å and 1°, respectively. The unit-cell parameters refined for pyromorphite agree with the reference within 0.01 Å. The unit-cell parameters for mimetite agree with those reported by Calos & Kennard (1990) within 0.002 Å. Unit-cell dimensions

Table 4
Atomic coordinates and equivalent isotropic displacement factors in minerals from the pyromorphite–mimetite series.

	Sample ID										
Atom	0	0.1	0.2	0.3	0.4	0.5	0.6	0.7	0.8	0.9	1
Pb1 *x*	0.3333	0.3333	0.3333	0.3333	0.3333	0.3333	0.3333	0.3333	0.3333	0.3333	0.3333
Pb1 *y*	0.6666	0.6666	0.6666	0.6666	0.6666	0.6666	0.6666	0.6666	0.6666	0.6666	0.6666
Pb1 *z*	0.00411 (10)	0.00413 (13)	0.00374 (18)	0.00400 (15)	0.00463 (19)	0.00426 (16)	0.50480 (15)	0.50518 (14)	0.50574 (15)	0.50537 (14)	0.5062 (12)
Pb1 U_{iso}(Å)	0.0154 (07)	0.0172 (1)	0.0191 (1)	0.0211 (1)	0.0193 (1)	0.0221 (1)	0.0173 (1)	0.0193 (1)	0,0172 (1)	0.0175 (1)	0.0180 (1)
Pb2 *x*	0.25471 (4)	0.25447 (5)	0.25417 (6)	0.25365 (6)	0.25364 (7)	0.25309 (6)	0.25282 (5)	0.25251 (6)	0.25196 (6)	0.25161 (6)	0.25085 (5)
Pb2 *y*	0.00582 (6)	0.00623 (7)	0.00634 (9)	0.00564 (8)	0.00653 (10)	0.00586 (8)	0.00612 (8)	0.00613 (8)	0.00573 (9)	0.00557 (9)	0.00454 (7)
Pb2 *z*	0.25000	0.2500	0.2500	0.2500	0.2500	0.2500	0.2500	0.2500	0.2500	0.2500	0.2500
Pb2 U_{iso}(Å)	0.01501 (6)	0.01708 (7)	0.01902 (11)	0.02121 (8)	0.01907 (12)	0.02204 (9)	0.01803 (11)	0.01919 (10)	0.01823 (12)	0.01907 (13)	0.01842 (9)
B† *x*	0.41023 (21)	0.40955 (22)	0.40923 (25)	0.40926 (22)	0.40874 (22)	0.40838 (19)	0.40903 (15)	0.40882 (15)	0.40869 (16)	0.40865 (15)	0.40863 (11)
B y	0.37900 (22)	0.37861 (23)	0.37872 (26)	0.37955 (23)	0.38056 (22)	0.38094 (19)	0.38187 (15)	0.38234 (15)	0.38263 (16)	0.38372 (15)	0.38440 (11)
B z	0.25000	0.25000	0.2500	0.2500	0.2500	0.2500	0.2500	0.2500	0.2500	0.2500	0.2500
B U_{iso}(Å)	0.00926 (65)	0.00620 (70)	0.00757 (83)	0.0149 (7)	0.0050 (7)	0.0137 (4)	0.0059 (4)	0.0070 (3)	0.0091 (5)	0.0100 (4)	0.0087 (8)
O1 *x*	0.3420 (6)	0.3438 (7)	0.3436 (9)	0.3410 (9)	0.3388 (10)	0.3378 (9)	0.3336 (8)	0.3304 (8)	0.3268 (9)	0.3225 (9)	0.3257 (7)
O1 *y*	0.4877 (5)	0.4889 (7)	0.4907 (8)	0.4920 (8)	0.4908 (9)	0.4924 (8)	0.4941 (8)	0.4932 (8)	0.4944 (9)	0.4934 (9)	0.4910 (7)
O1 *z*	0.2500	0.2500	0.2500	0.2500	0.2500	0.2500	0.2500	0.2500	0.2500	0.2500	0.2500
O1 U_{iso}(Å)	0.0135 (13)	0.0314 (25)	0.0393 (35)	0.0297 (24)	0.0443 (44)	0.0425 (28)	0.0405 (37)	0.0324 (26)	0.0223 (29)	0.0215 (36)	0.0222 (21)
O2 *x*	0.5879 (5)	0.5892 (6)	0.5913 (8)	0.5895 (8)	0.5936 (9)	0.5941 (8)	0.5965 (7)	0.5955 (7)	0.5989 (9)	0.5975 (9)	0.5991 (7)
O2 *y*	0.4735 (5)	0.4747 (6)	0.4757 (8)	0.4752 (8)	0.4795 (9)	0.4811 (8)	0.4828 (7)	0.4847 (7)	0.4865 (8)	0.4863 (9)	0.4872 (7)
O2 *z*	0.2500	0.2500	0.2500	0.2500	0.2500	0.2500	0.2500	0.2500	0.2500	0.2500	0.2500
O2 U_{iso}(Å)	0.0064 (11)	0.0123 (19)	0.0152 (26)	0.0219 (21)	0.0166 (30)	0.0232 (23)	0.00931 (23)	0.0135 (20)	0.0145 (24)	0.0209 (33)	0.0246 (21)
O3 *x*	0.35943 (33)	0.3586 (4)	0.3590 (5)	0.3586 (6)	0.3574 (6)	0.3584 (5)	0.3583 (5)	0.3575 (5)	0.3581 (6)	0.3579 (6)	0.3579 (5)
O3 *y*	0.2717 (4)	0.2708 (4)	0.2717 (5)	0.2698 (6)	0.2709	0.2686 (5)	0.2699 (5)	0.2708 (5)	0.2713 (6)	0.2702 (6)	0.2694 (6)
O3 *z*	0.0798 (4)	0.0786 (5)	0.0789 (6)	0.0777 (7)	0.0774	0.0747 (6)	0.0725 (6)	0.0722 (6)	0.0688 (8)	0.0682 (7)	0.0683 (7)
O3 U_{iso}(Å)	0.0128 (9)	0.02298 (165)	0.0208 (20)	0.0188 (13)	0.0242 (24)	0.0276 (16)	0.0288 (21)	0.0276 (16)	0.0332 (20)	0.0405 (29)	0.0444 (18)
Cl *x*	0.0000	0.0000	0.0000	0.0000	0.0000	0.0000	0.0000	0.0000	0.0000	0.0000	0.0000
Cl *y*	0.0000	0.0000	0.0000	0.0000	0.0000	0.0000	0.0000	0.0000	0.0000	0.0000	0.0000
Cl *z*	0.0000	0.0000	0.0000	0.0000	0.0000	0.0000	0.0000	0.0000	0.0000	0.0000	0.0000
Cl U_{iso}(Å)	0.0104 (5)	0.0132 (8)	0.0149 (11)	0.0174 (9)	0.0115 (12)	0.0174 (9)	0.0113 (10)	0.0121 (8)	0.0166 (11)	0.0181 (13)	0.0207 (9)

† $B = P^{5+}$ or As^{5+}.

Table 5
Selected mean bond lengths (Å) and bond angles (°) in minerals from the pyromorphite–mimetite series.

Sample ID As/(P + As)	Pb1—O	Pb2—O	*B*—O†	O1—*B*—O2	O3—*B*—O3
0	2.71 (03)	2.69 (05)	1.54 (06)	110.4 (3)	106.7 (2)
0.1	2.72 (05)	2.68 (05)	1.56 (07)	109.0 (3)	107.2 (3)
0.2	2.71 (06)	2.69 (07)	1.57 (09)	109.3 (4)	107.6 (4)
0.3	2.71 (05)	2.69 (07)	1.59 (08)	109.9 (4)	106.2 (3)
0.4	2.72 (06)	2.70 (08)	1.60 (10)	110.4 (4)	106.0 (4)
0.5	2.72 (05)	2.70 (07)	1.62 (08)	109.9 (4)	105.1 (3)
0.6	2.73 (05)	2.71 (04)	1.63 (08)	110.4 (3)	106.2 (3)
0.7	2.73 (05)	2.71 (05)	1.65 (07)	112.1 (4)	105.9 (3)
0.8	2.74 (06)	2.72 (06)	1.66 (08)	111.8 (4)	106.2 (4)
0.9	2.74 (06)	2.72 (08)	1.68 (08)	113.2 (4)	105.5 (4)
1	2.75 (05)	2.73 (05)	1.69 (05)	113.3 (2)	105.8 (3)

† $B = P^{5+}$ or As^{5+}.

for this mineral reported by Dai *et al.* (1991) are 0.04 Å shorter.

All of the solid solutions, with analogy to pyromorphite and mimetite, were found to crystallize in space group $P6_3/m$. The reader is asked to refer to the paper by Mercier *et al.* (2005) where the structure of $P6_3/m$ apatites is reported in detail. The goal of this study was to determine the range and the structural impact of low-temperature anionic substitutions within the minerals from the pyromorphite–mimetite series. Thus, only the structural changes caused by anionic substitutions will be described in detail. Refined chemical compositions of particular phases (Table 3) confirmed the results of classical wet chemical analyses as well as SEM-EDS characterization of the solids. These were also in agreement with anionic proportions intended during the synthesis. It proves that at low temperatures no crystal-chemical limitations for As^{5+}–P^{5+} substitutions within pyromorphite and mimetite structures can be found. The series is continuous and the tetrahedral substitutions within depend only on thermodynamic equilibrium in the environment.

The major structural differences in minerals from the pyromorphite–mimetite series occur in the BO_4 tetrahedra, in which *B* is occupied by substituting As^{5+}(0.46 Å radius) and P^{5+} (0.17 Å radius). As presented in Fig. 4, there is an increasing trend in *B*—O bond lengths with progressive anionic substitutions. The more As^{5+} compound in the structure, the longer the mean *B*—O distances within tetrahedra are observed. The variation in O1—*B*—O2 bond symmetry with anionic substitutions is apparent. The distortion of O1—*B*—O2 bond symmetry increases with complexity of the chemical composition of the solids. As indicated by infrared spectroscopy analysis of the precipitates, changes in tetrahedra symmetry occur mainly in PO_4^{3-} tetrahedra. The distortion of PO_4^{3-} symmetry increases with progressive anionic substitution. Local symmetry of the larger in size AsO_4^{3-} tetrahedra, however, remains unchanged. Thus, the greatest symmetry distortion of the O1—*B*—O2 bond is observed for the solid solution in which 50% of PO_4^{3-} tetrahedra are substituted.

The variation in the unit-cell dimensions with chemical composition of phases within the series is also observed. The more As^{5+} compound in the structure, the larger the unit cell, and greater *a* and *c* lattice parameters were refined (Figs. 5*a* and 5*b*). As suggested by Dai & Hughes (1989), the substitutions in BO_4 cause *a* to vary, mainly by differences in *B*—O1 and *B*—O2 bond lengths between PO_4 and AsO_4 tetrahedra. In apatites with $P6_3/m$ symmetry the *B*—O1 and *B*—O2 bonds lie in the mirror plane, parallel to [001]. The *B*—O3 bonds are about 55° from the [001] plain. Thus differences in *B*—O3 bond lengths between substituted tetrahedra respond in variation of the *c* lattice parameter. Figs. 6(*a*) and 6(*b*) present the correlation between particular *B*—O bonds lengths and

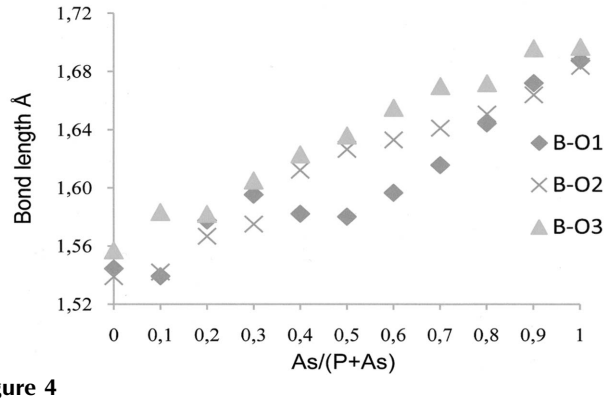

Figure 4
Variation in tetrahedra BO_4 bond lengths with chemical composition of the minerals from the pyromorphite–mimetite series.

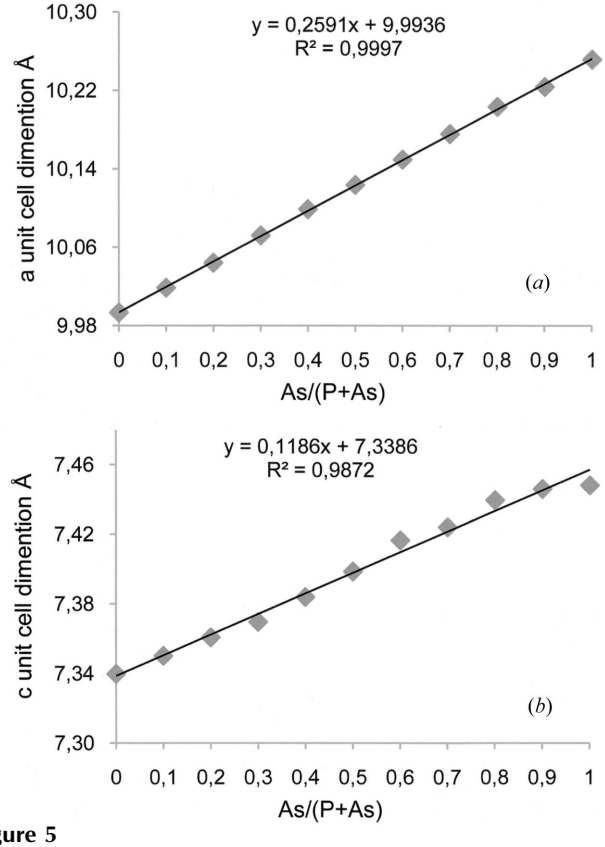

Figure 5
Variation in structural parameters according to composition: (*a*) variation in the *a* parameter, (*b*) variation in the *c* parameter.

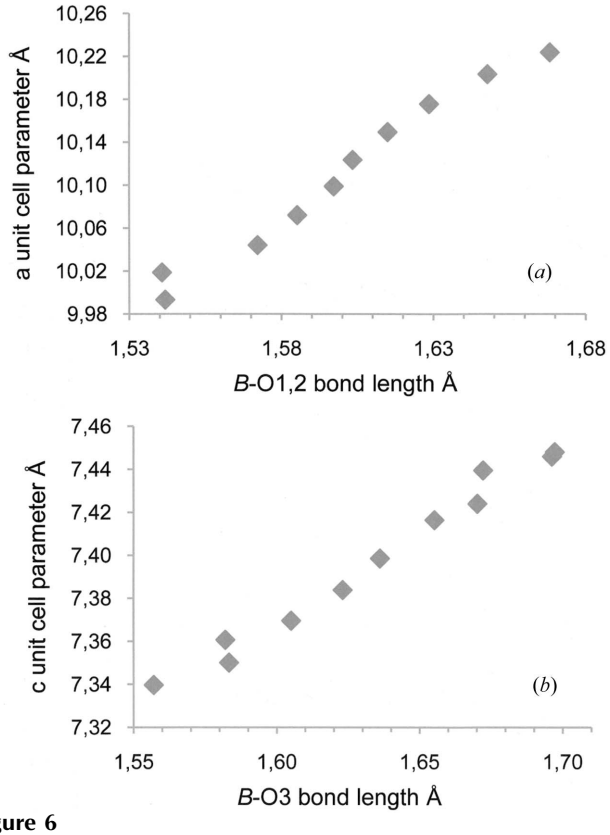

Figure 6
Correlation between the unit-cell dimensions and BO_4 tetrahedra bond lengths in minerals from the pyromorphite–mimetite series: (*a*) correlation between *a* parameter and *B*—O1,2 mean bond lengths, (*b*) correlation between *c* parameter and *B*—O3 bond lengths. The calculated correlation coefficients are equal to 0.99 in both cases.

a and *c* unit-cell parameters, respectively. In general, 10% substitution of As^{5+} for P^{5+} within tetrahedra causes on average a change of 0.029 Å in *B*—O(1,2) and 0.014 Å in *B*—O3 bond lengths. This is accompanied by 0.026 Å and 0.01 Å changes in *a* and *c* parameters, respectively. The differences in tetrahedral *B*—O bond lengths are confirmed to be the main factors affecting *a* and *c* unit-cell parameters of minerals of the pyromorphite–mimetite series. More detailed interpretation of structural changes caused by tetrahedra substitutions, however, can be derived from a model proposed by Mercier *et al.* (2005). It has been reported that the *c* and *a* unit-cell dimensions of $P6_3/m$ apatites can be reproduced from crystal-chemical parameters characterizing ...–Pb2–O3–*B*–O3–Pb2–... atom chains and (Pb1–O6)–(BO_4) polyhedral arrangements, respectively. Based on this model it can be assumed that tetrahedral substitutions within the pyromorphite–mimetite series, in addition to variations in *B*—O bond lengths, cause some minor rearrangements in Pb—O bond lengths and angles. The variations in Pb—O bond lengths and angles as well as variation in O—*B*—O bond angles with changes in chemical composition of phases within the series are presented in Figs. 7(*a*) and 7(*b*). In terms of structural changes along the *c* parameter indeed some small variation in ...–Pb2–O3–*B*–O3–Pb2–... atom chains can be observed. Progressive substitution of the larger tetrahedra and elongation of the *B*—O3 bond are accompanied by a minor decrease in the O3—*B*—O3 bond angle. This influences the Pb2—O3 bond by increasing the distance between atoms and diminishing the angle O3—Pb2—O3. Structural rearrangements in the [001] plain owing to the tetrahedra substitution are more complex. Unlike the O3—*B*—O3 bond angle, the O1—*B*—O2 angle increases with progressive tetrahedral substitution. There are differences in response of particular Pb1—O bonds to this change and as a result minor rearrangement within the (Pb1—O6) polyhedron occurs. The Pb1—O1 bond shortens with As^{5+} substitutions while the Pb1—O2 bond lengthens. Considered by White & ZhiLi (2003) as a qualitative predictor

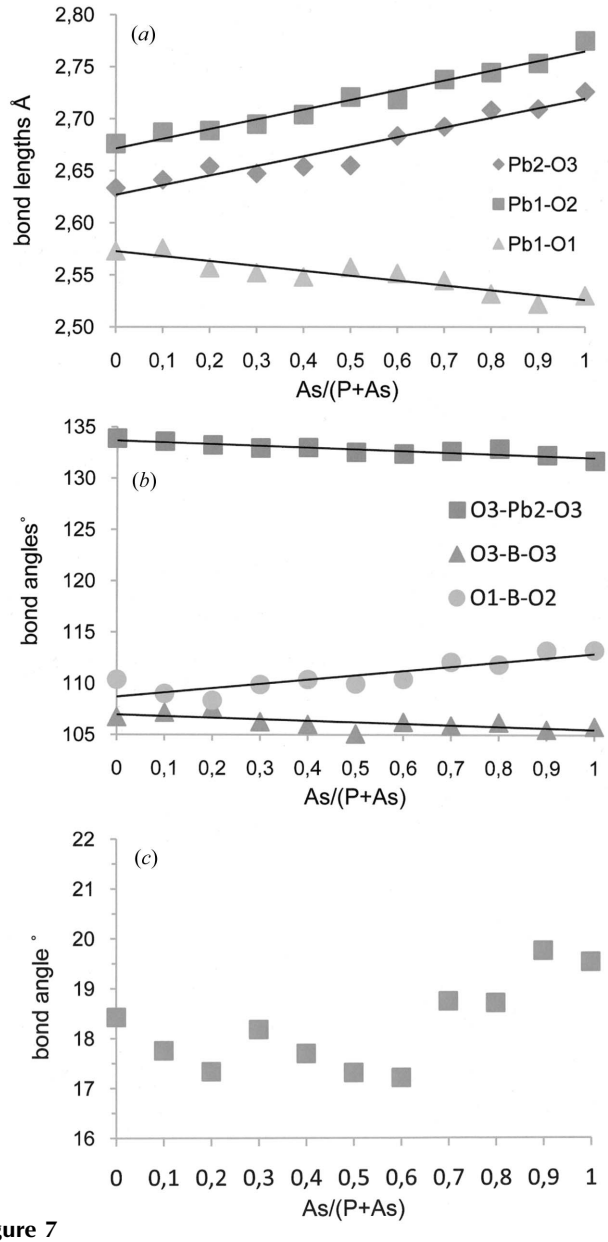

Figure 7
Variation in selected bond lengths and angles from ...–Pb2–O3–*B*–O3–Pb2–... atom chains and (Pb1–O6)–(BO_4) polyhedral with chemical composition of the minerals from the pyromorphite–mimetite series: (*a*) variation in selected bond lengths, (*b*) variation in selected bond angles, (*c*) variation in the metaprism twist angle φ in O1—Pb1—O2, defined by White & ZhiLi (2003).

of the apatite distortion, the metaprism twist angle φ in the O1—Pb1—O2 bond varies minutely with progressive tetrahedral substitutions; however, the trend or the dependence of the variation cannot be determined (Fig. 7*c*).

The unit-cell parameters of pyromorphite, mimetite and their solid solutions refined in this study agree well with those of previous synthetic compounds prepared as single crystals or fine powders at high temperatures (Baker, 1966; Masaoka *et al.*, 2006). The dependency between chemical composition of the phases and the unit-cell parameters is completely linear from pyromorphite to mimetite (Fig. 5). It proves that in terms of occupancy all of the tetrahedra sites are equal within the structure and no preferred occupancy occurs.

4. Summary

The use of the dedicated high-resolution high-throughput diffraction beamline 11-BM allowed for quick collection of data of a quality unavailable on any conventional radiation source. Superior resolution achieved on this state-of-the-art instrument was essential in the study of the pyromorphite–mimetite solid solution series, which is prone to severe peak overlapping and characterized by subtle structural changes among adjacent members. The characteristics of the synchrotron radiation allowed also for the detection of impurities within analyzed solids, undetectable by other methods.

Structural Rietveld refinement of the synchrotron-based data allowed for precise determination of structural parameters of minerals from the pyromorphite–mimetite series, including anionic site occupancies. The refined compositions are in good agreement with the theoretical composition of the samples based on the chemistry of the starting solutions. The results of the structural Rietveld refinement confirmed that the pyromorphite–mimetite solid solution series is complete at low temperatures and that tetrahedral cation sites, occupied by substituting As^{5+} and P^{5+}, are single and crystallographically unique. The differences in B—O1 and B—O2 bond lengths between PO_4 and AsO_4 tetrahedra are responsible for the variations in the *a* unit-cell dimensions for phases with different chemical composition. Changes in the *c* parameter, on the other hand, are due to the differences in B—O3 tetrahedra bond lengths. Some minor structural rearrangements within ...–Pb2–O3–*B*–O3–Pb2–... atom chains and (Pb1–O6)–(BO_4) polyhedra caused by anionic substitutions within the pyromorphite–mimetite series were reported.

We gratefully acknowledge support of the MNiSZW through grant N N307 101535. We are also thankful to Dr Marta Strycharczyk for rendering samples and results of the EDS analysis accessible.

References

Baker, W. E. (1966). *Am. Mineral.* **51**, 1712–1721.
Calos, N. J. & Kennard, C. H. L. (1990). *Z. Kristallogr.* **191**, 125–129.
Dai, Y. & Hughes, J. M. (1989). *Can. Mineral.* **27**, 189–192.
Dai, Y., Hughes, J. M. & Moore, P. B. (1991). *Can. Mineral.* **29**, 369–376.
Finger, L. W., Cox, D. E. & Jephcoat, A. P. (1994). *J. Appl. Cryst.* **27**, 892–900.
Frost, R. L., Reddy, B. J. & Palmer, S. J. (2008). *Polyhedron*, **27**, 1747–1753.
Larson, A. C. & Von Dreele, R. B. (2000). *General Structure Analysis System (GSAS)*. LANL Report No. LAUR 86–748. Los Alamos National Laboratory, NM, USA.
Lee, P. L., Shu, D., Ramanathan, M., Preissner, C., Wang, J., Beno, M. A., Von Dreele, R. B., Ribaud, L., Kurtz, C., Antao, S. M., Jiao, X. & Toby, B. H. (2008). *J. Synchrotron Rad.* **15**, 427–432.
Lenoble, V., Deluchat, V., Serpaud, B. & Bollinger, J. C. (2003). *Talanta*, **61**, 267–276.
Ma, Q. Y., Traina, S. J., Logan, T. J. & Ryan, J. A. (1993). *Environ. Sci. Technol.* **27**, 1830–1850.
Masaoka, M., Kyono, A., Hatta, T. & Kimata, M. (2006). *J. Cryst. Growth*, **292**, 129–135.
Mercier, P. H. J., Le Page, Y., Whitfield, P. S., Mitchell, L. D., Davidson, I. J. & White, T. J. (2005). *Acta Cryst.* B**61**, 635–655.
Nakamoto, A., Urasima, Z., Sugiura, S., Nakano, H., Yachi, T. & Tadokoro, K. (1969). *Jpn. Mineral. J.* **6**, 85–101.
Nakamoto, K. (1986). *Infrared and Raman Spectra of Inorganic and Coordination Compounds*, Vol. 4, p. 496. New York: Wiley Interscience.
Pan, Y. & Fleet, M. E. (2002). *Phosphates: Geochemical, Geobiological, and Materials Importance*, Vol. 48, *Reviews in Mineralogy and Geochemistry*, edited by M. J. Kohn, J. Rakovan and J. M. Hughes, pp. 13–49. Washington: Mineralogical Society of America.
Rajan, K. K. & Lim, L. C. (2003). *Appl. Phys. Lett.* **83**, 5277–5279.
Ruby, M. V., Davis, A. & Nicholson, A. (1994). *Environ. Sci. Technol.* **28**, 646–654.
Stephens, P. W. (1999). *J. Appl. Cryst.* **32**, 281–289.
Thompson, P., Cox, D. E. & Hastings, J. B. (1987). *J. Appl. Cryst.* **20**, 79–83.
Toby, B. H. (2001). *J. Appl. Cryst.* **34**, 210–213.
Wang, J., Toby, B. H., Lee, P. L., Ribaud, L. R., Antao, S. M., Kurtz, Ch., Ramanathan, M., Von Dreele, R. B. & Beno, M. A. (2008). *Rev. Sci. Instrum.* **79**, 085105.
White, T. J. & ZhiLi, D. (2003). *Acta Cryst.* B**59**, 1–16.